Characterization of the Preferred Stereochemistry for the Neuropharmacologic Actions of Antillatoxin

7 AUTHORS, INCLUDING:

Fumiaki Yokokawa
Novartis
68 PUBLICATIONS   **1,388** CITATIONS

William Gerwick
University of California, San Diego
393 PUBLICATIONS   **11,313** CITATIONS

Thomas F Murray
Creighton University
209 PUBLICATIONS   **4,802** CITATIONS

Characterization of the Preferred Stereochemistry for the Neuropharmacologic Actions of Antillatoxin

W. I. Li,[†] B. L. Marquez,[‡] T. Okino,[‡] F. Yokokawa,[§] T. Shioiri,[§] W. H. Gerwick,*[,‡] and T. F. Murray*[,†]

Department of Physiology and Pharmacology, College of Veterinary Medicine, University of Georgia, Athens, Georgia 30602-7389, College of Pharmacy, Oregon State University, Corvallis, Oregon 97331, and Faculty of Pharmaceutical Sciences, Nagoya City University, Nagoya 4678603, Japan

Antillatoxin is a potent ichthyotoxin and cytotoxin previously discovered from the marine cyanobacterium *Lyngbya majuscula*. Ensuing studies of its mechanism of action showed it to activate the mammalian voltage-gated sodium channel at a pharmacological site that is distinct from any previously described. The structure of antillatoxin, initially formulated from spectroscopic information, was subsequently corrected at one stereocenter (C-4) as a result of synthesis of four different antillatoxin stereoisomers (all possible C-4 and C-5 diastereomers). In the current study these four stereoisomers, (4*R*,5*R*)-, (4*S*,5*R*)-, (4*S*,5*S*)-, and (4*R*,5*S*)-antillatoxin, were characterized in five different biological assay systems: ichthyotoxicity to goldfish, microphysiometry using cerebellar granule cells (CGCs), lactose dehydrogenase efflux from CGCs, monitoring of intracellular Ca^{2+} concentrations in CGCs, and cytotoxicity to Neuro 2a cells. Across these various biological measures there was great consistency in that the natural antillatoxin (the 4*R*,5*R*-isomer) was greater than 25-fold more potent than any of the other stereoisomers. Detailed NMR studies provided a number of torsion and distance constraints that were modeled using the MM2* force field to yield predicted solution structures of the four antillatoxin stereoisomers. The macrocycle and side chain of natural (4*R*,5*R*)-antillatoxin present an overall "L-shaped" topology with an accumulation of polar substituents on the external surface of the macrocycle and a hydrogen bond between N(H)-7′ and the C(O)-1 carbonyl. The decreased potency of the three non-naturally occurring antillatoxin stereoisomers is certainly a result of their dramatically altered overall molecular topologies.

Marine cyanobacteria (blue-green algae) are prolific producers of structurally novel and biologically active natural products and are especially rich in metabolites, which combine amino acid and polyketide portions to form mixed biogenesis metabolites.[1] The ranges in biological activity are vast and include anticancer compounds such as curacin A,[2] neurotoxins such as kalkitoxin,[3] antifungal agents such as hectochlorin,[4] and cytotoxins that work by as yet unknown mechanisms such as apratoxin.[5]

Antillatoxin (ATX) is a structurally novel lipopeptide produced by the pantropical marine cyanobacterium *Lyngbya majuscula*.[6] Blooms of *L. majuscula* have been associated with adverse effects on human health, including respiratory irritation, eye inflammation, and severe contact dermatitis in exposed individuals. ATX has been reported to be among the most ichthyotoxic metabolites isolated to date from a marine microalga and is exceeded in potency only by the brevetoxins.[6]

Using cerebellar granule cells, we have shown that ATX produces neuronal death, which is prevented by co-application of an NMDA receptor antagonist.[7] This neurotoxic effect of ATX is also antagonized by tetrodotoxin, which suggested an interaction of ATX with voltage-gated sodium channels (VGSC).[8] ATX-induced stimulation of Ca^{2+} influx in cerebellar granule cells was similarly prevented by tetrodotoxin. Additional, more direct, evidence for the VGSC serving as the molecular target for ATX was provided by the demonstration of ATX stimulation of [³H]-batrachotoxin binding and ²²Na$^+$ influx in cerebellar granule cells.[8] Together these results establish ATX as a novel

activator of VGSC. The precise recognition site for ATX on the VGSC, however, remains to be defined.

The original planar structure of antillatoxin was assembled via standard spectroscopic techniques, while stereochemistry of the two optically active amino acids was accomplished by chiral TLC analysis, revealing an *S* stereochemistry at both α-carbons. The stereochemistry of C-4 and C-5 was characterized by a combination of homonuclear dipolar and scalar coupling interactions, circular dichroism (CD) spectroscopy, and molecular modeling.[6] Interpretation of these spectroscopic data initially indicated that the absolute stereochemistry of antillatoxin was 4*S*,5*R*,2′*S*,5′*S*. However, spectroscopic data obtained from a synthetic sample of this isomer showed this to be incorrect, and this led to a synthetic project to synthesize all four C-4 and C-5 stereoisomers of antillatoxin, clarifying the natural structure as the (4*R*,5*R*)-isomer (Figure 1).[9]

The objective of the present study was to define the preferred C-4 and C-5 stereochemistry for the pharmacologic actions of ATX in cerebellar granule cells. The role of these two asymmetric carbon atoms in the interaction of ATX with its molecular target was assessed through a pharmacologic characterization of the four ATX isomers. These results indicate that the preferred configuration for ATX-induced alterations in neuronal signaling is presented by the natural (4*R*,5*R*)-isomer. Detailed NMR analyses were used to provide numerous distance and torsion angle restraints in the molecular modeling of each of the four tested antillatoxin stereoisomers, thereby leading to an initial characterization of the molecular determinants for antillatoxin interaction with its neuroreceptor target.

Results and Discussion

Cytotoxicity. We have previously reported that the naturally occurring (−)-ATX produced substantial neuronal death in CGC cultures exposed for 2 h.[7,8] This cytotoxic

* To whom correspondence should be addressed. (Chemistry) Tel: 541-737-5801. Fax: 541-737-3999. E-mail: Bill.Gerwick@oregonstate.edu. (Pharmacology) Tel: 706-542-3014. Fax: 706-542-3015. E-mail: Tmurray@vet.uga.edu.
† University of Georgia.
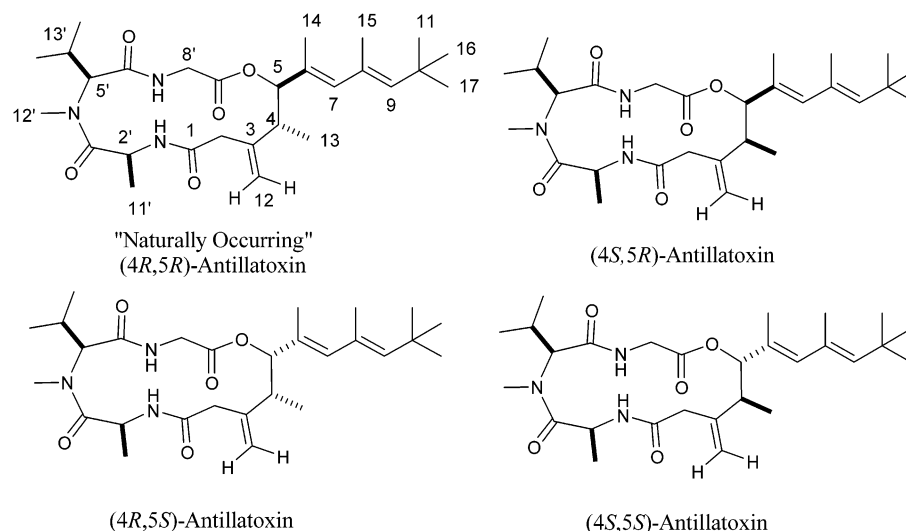‡ Oregon State University.
§ Nagoya City University.

"Naturally Occurring"
(4*R*,5*R*)-Antillatoxin

(4*S*,5*R*)-Antillatoxin

(4*R*,5*S*)-Antillatoxin

(4*S*,5*S*)-Antillatoxin

Figure 1. Four possible stereoisomers about the C-4−C-5 bond of antillatoxin.

Table 1. Biological Evaluation of Antillatoxin Stereoisomers for Ichthyotoxicity, Neurotoxicity, and Extracellular Acidification Rate (microphysiometry)

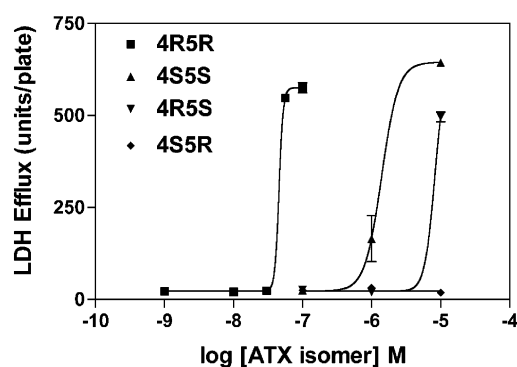| stereoisomer	ichthyotoxicity	microphysiometry	LDH assay	neuro 2a assay
4*R*,5*R*	ca. 0.1 μM	41 nM	42 nM	0.18 μM
4*S*,5*S*	slight at 10 μM	5−10 μM	1.4 μM	5−10 μM
4*R*,5*S*	inactive at 10 μM	5−10 μM	8.1 μM	ca. 10 μM
4*S*,5*R*	slight at 10 μM	inactive	inactive	ca. 10 μM

Figure 2. Neurotoxic concentration−response profiles of 11−13 days in culture rat cerebellar granule cells exposed 2 h to antillatoxin stereoisomers. Exposure conditions and LDH determination were as described in the Experimental Section. Individual points represent mean − SEM from two separate experiments each performed in triplicate.
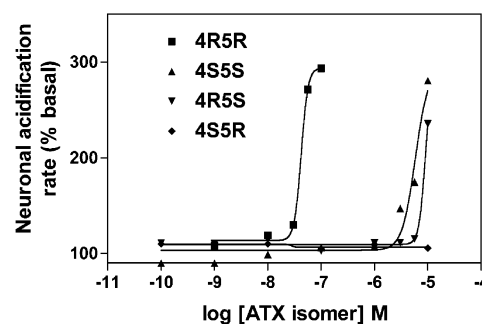

Figure 3. Antillatoxin stereoisomer concentration−response profiles for stimulation of extracellular acidification rate in cerebellar granule cells. Neurons were cultured on porous polycarbonate membranes, and acidification rate was monitored by microphysiometry as described in the Experimental Section. Peak acidification rates are expressed as a percentage of basal proton efflux. Individual points represent the mean − SEM from two separate experiments each performed in duplicate.

response was reflected in elevated LDH efflux into the culture medium. Co-incubation of ATX (100 nM) with tetrodotoxin (1 μM) eliminated ATX neurotoxicity, indicating that VGSCs served as the molecular target for this pharmacologic response.[8] The recently synthesized (4*S*,5*R*)-, (4*R*,5*R*)-, (4*S*,5*S*)-, and (4*R*,5*S*)-stereoisomers were therefore examined for cytotoxic potency.[9] The cytotoxic potencies of the four isomers differed significantly, with the naturally occurring (4*R*,5*R*)-configuration being the most potent with a pEC$_{50}$ value of 7.34 ± 0.01 (45.7 nM). As shown in Figure 2, the (4*R*,5*R*)-, (4*S*,5*S*)-, and (4*R*,5*S*)-isomers produced concentration-dependent increases in LDH efflux after 2 h of exposure, whereas neurons treated with the (4*S*,5*R*)-isomer were unaffected. The (4*R*,5*R*)-isomer was 31 and 182 times more potent than the (4*S*,5*S*)- and (4*R*,5*S*)-isomers, respectively (Table 1). In agreement with our previous reports, the cytotoxic response to 100 nM of (4*R*,5*R*)-ATX was completely prevented by co-incubation with 1 μM tetrodotoxin (data not shown).

Natural (4*R*,5*R*)-antillatoxin was the most potent of the four isomers to the mouse neuro 2a cell line, with an LD$_{50}$ = 0.18 μM. This was 25−50 times more potent than the next most active isomer, (4*S*,5*S*)-ATX. The remaining two stereoisomers, (4*S*,5*R*)- and (4*R*,5*S*)-ATX, were at least 50-fold less potent than the natural isomer in this cell line (Table 1).

Extracellular Acidification Rate. In an effort to assess the influence of ATX isomers on a functional response of CGCs, extracellular acidification rates of CGCs were evaluated using a Cytosensor microphysiometer. Three of the four ATX isomers tested produced rapid and dramatic increments in the neuronal extracellular acidification rates. The (4*R*,5*R*)-isomer was the most potent analogue tested, increasing the extracellular acidification rate by as much as 300% at a concentration of 100 nM (Figure 3). The (4*S*,5*R*)-isomer was again inactive, while the (4*S*,5*S*)- and (4*R*,5*S*)-isomers were active but much less potent than (4*R*,5*R*)-ATX. The pEC$_{50}$ values for these latter three ATX isomers were in remarkable agreement with
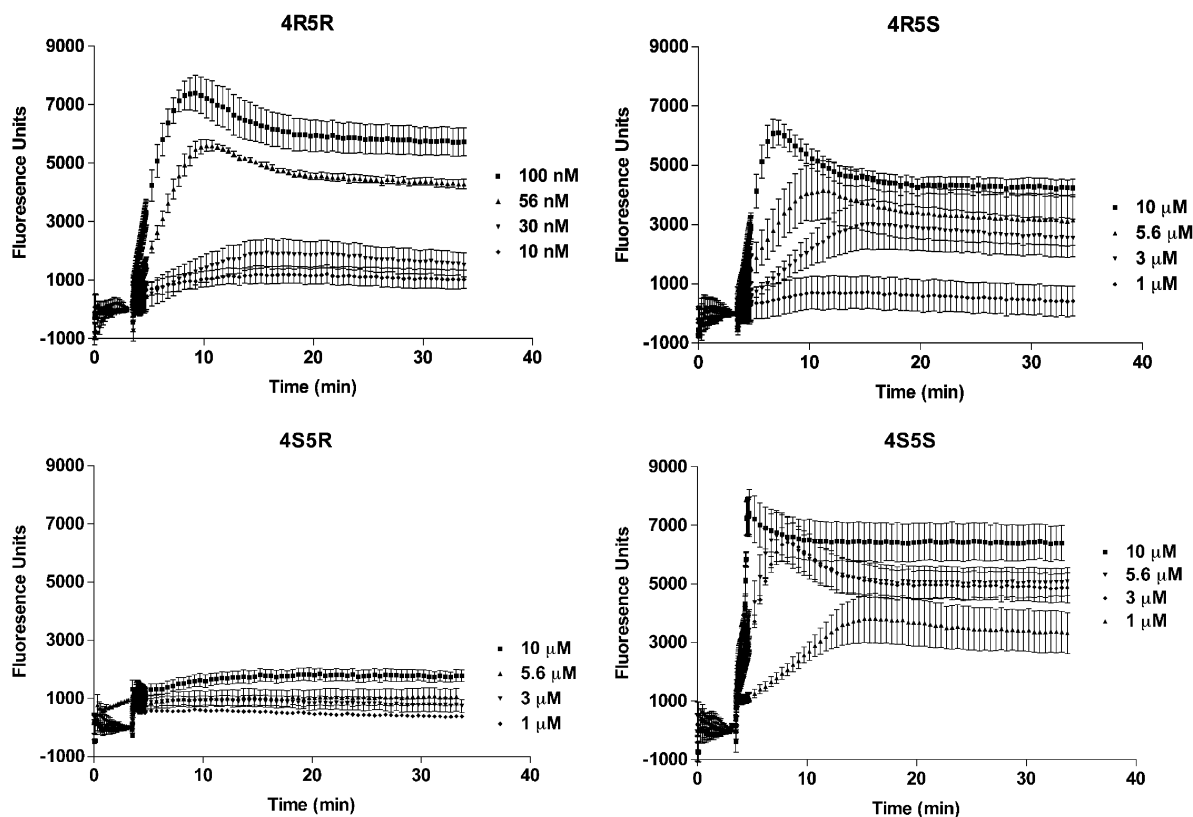
Figure 4. Increases in fluo-3 fluorescence detected by FLIPR in cerebellar granule cells exposed to antillatoxin stereoisomers. Data are from a representative experiment performed in quadruplicate and twice repeated. Basal fluo-3 fluorescence has been subtracted from each value and represented approximately 4000 fluorescence units.

those derived from the cytotoxicity assays. The $(4R,5R)$-isomer was accordingly found to be 135 and 209 times more potent than, respectively, the $(4S,5S)$- and $(4R,5S)$-isomers.

Ca²⁺ Influx. We have previously reported that CGCs treated with 100 nM ATX display a rapid increase in cytoplasmic [Ca²⁺], which is prevented by co-incubation with tetrodotoxin.[8] The ATX-induced Ca²⁺ influx is therefore triggered by activation of VGSC with resultant activation of voltage-gated Ca²⁺ channels, reversal of the Na⁺−Ca²⁺ exchanger, and/or relief of the voltage-dependent block of NMDA receptors by Mg²⁺.[8] The configurational preference for the Ca²⁺ response was therefore explored. As depicted in Figure 4, all four ATX isomers produced concentration- and time-dependent increases in cytoplasmic [Ca²⁺] as monitored by fluo-3 fluorescence. The stereoselective behavior of the four isomers differed with respect to both potency and efficacy. The $(4R,5R)$-isomer of ATX was 36 and 89 times more potent than, respectively, the $(4S,5S)$- and $(4R,5S)$-isomers (Figure 5). Although concentrations of 1−10 μM of $(4S,5R)$-ATX produced small, but detectable, increments in cytoplasmic [Ca²⁺], these data were insufficient to permit calculation of pEC₅₀ values by nonlinear regression analysis with a logistic function. As revealed in Table 1, these stereochemical preferences for stimulation of Ca²⁺ influx accord favorably with those observed in effects on both cytotoxicity and acidification rate.

NMR Studies. Initial structural assignment of $4S,5R$ stereochemistry to antillatoxin, based on a combination of coupling constants and H-4 to H-5 NOE correlations in the magnitude mode NOESY, was in error.[6] The correct $4R,5R$ stereochemistry of natural antillatoxin was revealed by chemical synthesis of all four stereoisomers at C-4 and C-5.[9] Synthetic production of these antillatoxin stereoisomers, in multi-milligram quantities, allowed for a detailed struc-
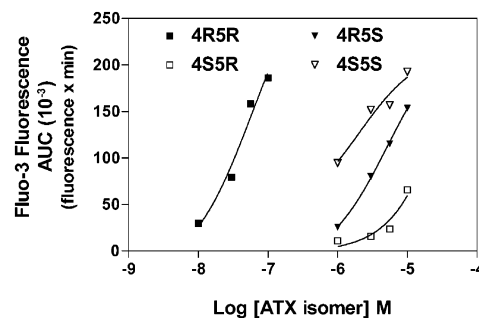

Figure 5. Antillatoxin stereoisomer concentration−response profiles for stimulation of Ca²⁺ influx in cerebellar granule cells. Each value is the mean integrated fluo-3 fluorescence response [area under the curve (AUC)] plotted as a function of each stereoisomer concentration.

tural and conformational analysis in addition to the pharmacological studies detailed above. The strategy for the structural analysis of these stereoisomers was to utilize first a suite of contemporary 2D NMR experiments to (a) make firm assignments of all ¹H and ¹³C NMR resonances [1D ¹H and ¹³C NMR, HSQC, and ¹H−¹H COSY], (b) accurately measure all homonuclear and heteronuclear coupling constants [E-COSY, HSQMBC], and (c) sensitively detect through-space proton−proton interactions without interference from scalar coupling artifacts [T-ROESY]. These data were utilized to provide restraints to a computed three-dimensional energy minimized conformation for each of the four stereoisomers.

In the original report of antillatoxin, chiral TLC methods were used to determine an S configuration for two of the four stereocenters in **6** ($2'S,5'S$). Following synthetic studies that showed natural antillatoxin to be of $4R,5R$ stereochemistry,[9] these two stereocenters were further investigated using additional NMR experiments. Indeed, a de-
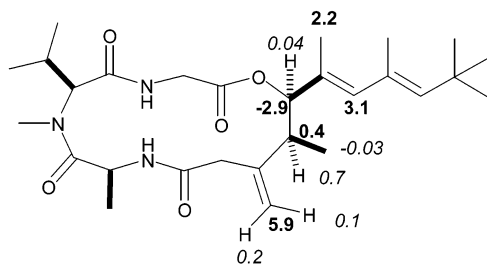
Figure 6. Originally proposed structure of antillatoxin with the incorrectly predicted 4S,5R stereochemistry. Values in bold represent $\Delta\delta$ values for (4S,5R)-antillatoxin ^{13}C NMR chemical shift − synthetic antillatoxin ^{13}C NMR shift. Values in italics indicate the $\Delta\delta$ values for (4S,5R)-antillatoxin ^{1}H NMR chemical shift − synthetic antillatoxin ^{1}H NMR shift.
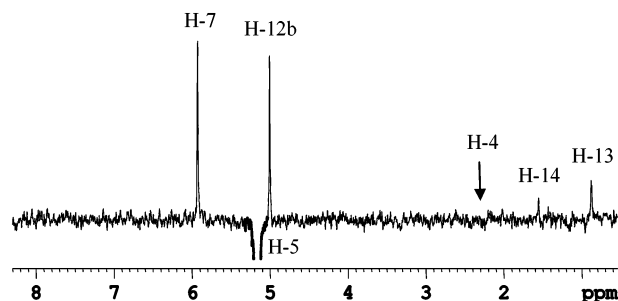

Figure 7. DPFGSE 1D NOE spectrum of natural antillatoxin with selective irradiation at H-5. The arrow indicates location of H-4 in the ^{1}H NMR spectrum.

tailed ^{1}H and ^{13}C NMR comparison of the synthetic 4S,5R material and natural antillatoxin revealed significant chemical shift discrepancies clustered around the C-4−C-5 region (Figure 6). Analysis of the original NOESY spectrum for natural antillatoxin revealed that these data were presented as a magnitude calculated spectrum, and thus, the NOE correlation between H-4 and H-5 was likely the result of a COSY (scalar coupling) artifact.[6] When H-5 was selectively irradiated using the DPFGSE 1D NOE experiment with a 60 ms Gaussian-shaped pulse,[10] only H-7, H-12b, H-13, and H-14 were enhanced (Figure 7). Critically, no enhancement of H-4 was observed, consistent with these protons existing on opposite faces of the macrocycle. With these new NMR data available, the original CD data could be reanalyzed to predict the correct 4R,5R stereochemistry.

The solution structure studies of each of the four antillatoxin stereoisomers were initiated with firm assignments of all ^{1}H and ^{13}C NMR resonances. This was accomplished via a combination of ^{1}H NMR, E-COSY,[11] and HSQMBC experiments.[12] Assignment of the diastereotopic protons at positions C2 and C8′ was achieved through simultaneous interpretation of dipolar couplings and the distance restrained model. In addition, the geminal protons at C-12 (H-12a and H-12b) were assigned on the basis of a combination of ROE data and measurement of $^3J_{CH}$ couplings. With all ^{1}H and ^{13}C NMR resonances assigned, dipolar coupling interactions, homonuclear couplings, and vicinal heteronuclear couplings were analyzed. The T-ROESY experiment, chosen to reduce strong scalar coupling artifacts that sometimes arise in the standard ROESY experiment, was used to analyze through-space interactions.[13] To deduce distance restraints, volumes of all correlations in the T-ROESY spectrum were integrated, normalized, and assigned values of strong (s), medium (m), and weak (w) as follows: s = 2 ± 1 Å, m = 2.5 ± 1.5 Å, and w = 3.0 ± 2 Å. ^{1}H NMR and E-COSY were used to measure $^3J_{HH}$ couplings, and the HSQMBC experiment was
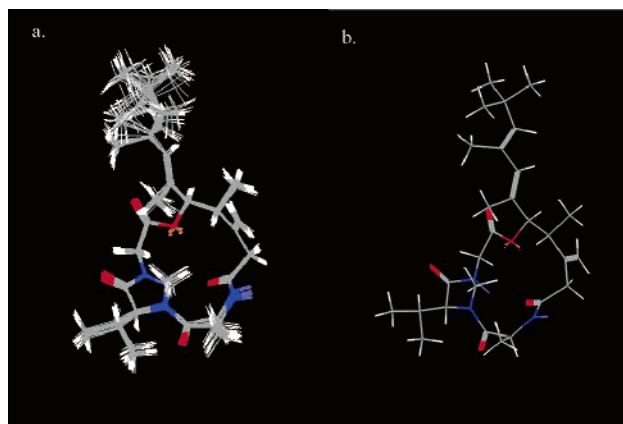

Figure 8. (a) Twenty overlaid structures taken from the Monte Carlo search of the constrained energy minimized structure of (4R,5R)-antillatoxin. (b) Lowest energy conformation of (4R,5R)-antillatoxin.

used to measure $^3J_{CH}$ coupling constants. The ϕ angles of the alanine residue and the diastereotopic protons of glycine were determined through measurement of $^3J_{NH-\alpha H}$ and the formula $^3J_{NH-\alpha H} = 6.7 \cos^2 \theta - 1.3 \cos \theta + 1.5$.[14] The ϕ angle was also calculated through measurement of the $^3J_{Ha-CO(i-1)}$ coupling constant and calculating a respective bond angle using the following Karplus equation: $^3J_{Ha-CO(i-1)} = 4.0 \cos^2 \theta - 1.8 \cos \theta + 0.18$.[15] To determine the angle χ of the N-Me valine residue, the $^3J_{H\beta-H\alpha}$ and $^3J_{H\beta-CO}$ coupling constants were measured and then used in the formula $^3J_{H\beta-H\alpha} = 6.7 \cos^2 \theta - 1.3 \cos \theta + 1.5$ and $^3J_{H\beta-CO} = 8.06 \cos^2 \theta - 0.87 \cos \theta + 0.47$.[16]

Molecular Modeling Calculations. Molecular modeling calculations were performed using Macromodel 7.0 utilizing the MM2* force field routine.[17] The molecular modeling was initiated by assembling the Dreiding model within Macromodel 7.0 and setting the stereochemistry at each of the four stereocenters. To derive the correct starting bond geometries, a steepest descent (SD) minimization with 100 iterations was performed using the MM2* force field. Distance constraints were entered into a constraint file within the minimization menu, and a 1000 iteration Polak-Ribier conjugate gradient (PRCG) minimization using the MM2* force field was performed.[18] The distance constrained model was then subjected to torsion angle constraints derived from $^3J_{HH}$ homonuclear and $^3J_{CH}$ heteronuclear coupling constants converted to their corresponding angles (calculated with the appropriate Karplus equation). Once all distance and torsion angle constraints were added, an additional PRCG minimization using the MM2* force field was performed. To further probe the available conformations within this minimum, a 1000-step Monte Carlo (MC) search was performed using the MM2* force field. Twenty of the lowest energy structures were overlaid for each of the four isomers and the rms deviations calculated (excluding all hydrogen atoms). For each antillatoxin isomer, the structures with the lowest energy minimum (determined several times throughout the calculation) from the constrained conformational searches are shown in Figures 8−12.

(4R,5R)-Antillatoxin (=Natural Antillatoxin). Table 2 tabulates the NMR data used to generate torsion angle and distance constraints for the molecular modeling calculations. A total of 22 distance and nine torsion angle constraints were used in the structure calculation. An error of ±20° was tolerated for the torsion angle parameters. The constrained model, using the MM2* force field, had a minimum energy of 258.73 kJ/mol. The MC search generated a new minimum of 255.45 kJ, which was found four
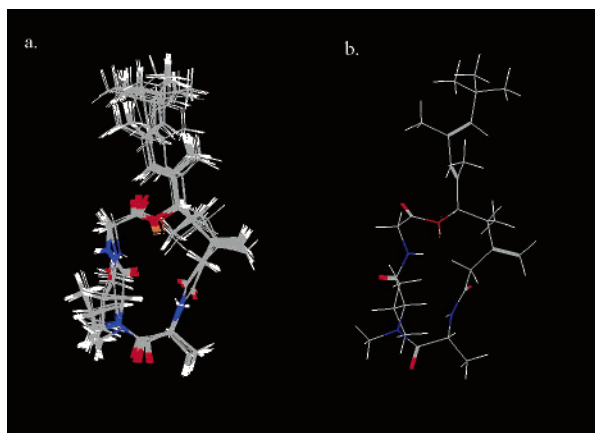
Figure 9. (a) Twenty overlaid structures taken from the Monte Carlo search of the constrained energy minimized structure (4*R*,5*S*)-antillatoxin. (b) Lowest energy conformation of (4*R*,5*S*)-antillatoxin.

Figure 10. (a) Twenty overlaid structures taken from the Monte Carlo search of the constrained energy minimized structure (4*S*,5*S*)-antillatoxin. (b) Lowest energy conformation of (4*S*,5*S*)-antillatoxin.
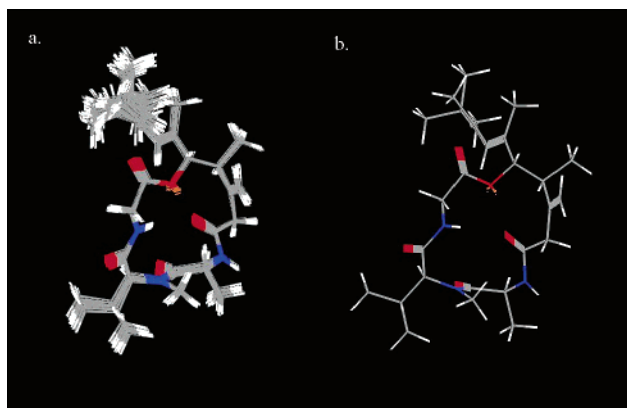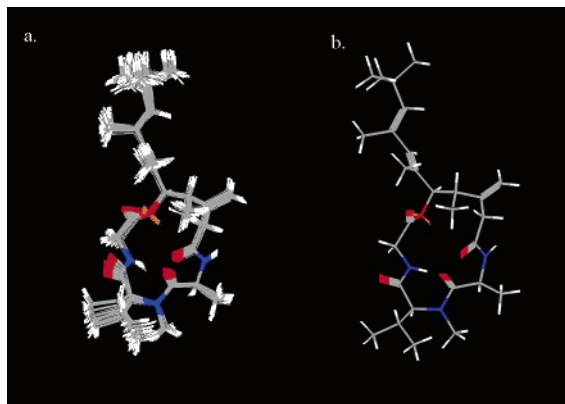

Figure 11. (a) Twenty overlaid structures taken from the Monte Carlo search of the constrained energy minimized structure (4*S*,5*R*)-antillatoxin. (b) Lowest energy conformation of (4*S*,5*R*)-antillatoxin.

times (Figure 8b). The 20 lowest energy structures were overlaid (Figure 8a), and an rms deviation was calculated using all non-hydrogen atoms. Of the 20 structures used for the calculation, the energy difference between the minimum and 20th structure was 1.12 kJ/mol. The rms deviation for these structures was 0.57 Å.

(4*R*,5*S*)-Antillatoxin. Table 3 tabulates the NMR data used to generate torsion angle and distance constraints for the molecular modeling calculations for the (4*R*,5*S*)-isomer. A total of 16 distance and seven torsion angle constraints were used in the structure calculation. An error of ±20° was tolerated for the torsion angle parameters. The con-
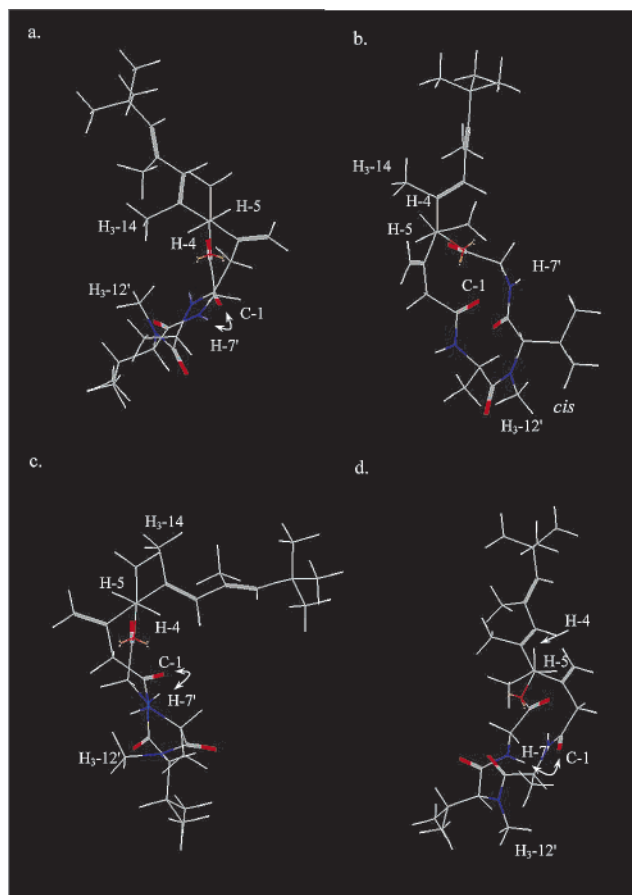

Figure 12. All models are displayed looking down the C-4−C-5 bond axis. (a) Lowest energy conformation of (4*R*,5*R*)-antillatoxin. (b) Lowest energy conformation of (4*R*,5*S*)-antillatoxin. (c) Lowest energy conformation of (4*S*,5*S*)-antillatoxin. (d) Lowest energy conformation of (4*S*,5*R*)-antillatoxin.

strained model, using the MM2* force field, had a minimum energy of 284.32 kJ/mol. The MC search generated a new minimum of 259.36 kJ, which was found 16 times (Figure 9b). The 20 lowest energy structures were overlaid (Figure 9a), and an rms deviation was calculated using all non-hydrogen atoms. Of the 20 structures used for the calculation, the energy difference between the minimum and structure 20 was 0.72 kJ/mol. The rms deviation for the 20 isomers was 0.77 Å.

(4*S*,5*S*)-Antillatoxin. Table 4 tabulates the NMR data used to generate the torsion angle and distance constraints for the molecular modeling calculations for the (4*S*,5*S*)-isomer. A total of 18 distance constraints and 12 torsion angle constraints were used in the structure calculation. An error of ±20° was tolerated for the torsion angle parameters. The constrained model, using the MM2* force field, had a minimum energy of 254.89 kJ/mol. The MC search generated a new minimum of 252.64 kJ, which was found three times (Figure 10b). The 20 lowest energy structures were overlaid (Figure 10a), and an rms deviation was calculated using all non-hydrogen atoms. Of the 20 structures used for the calculation, the energy difference between the minimum and structure 20 was 0.89 kJ/mol. The rms deviation for the 20 isomers was 0.49 Å.

(4*S*,5*R*)-Antillatoxin. Table 5 tabulates the NMR data used to generate the torsion angle and distance constraints for the molecular modeling calculations for the (4*S*,5*R*)-isomer. A total of 29 distance constraints and seven torsion angle constraints were used in the structure calculation. An error of ±20° was tolerated for the torsion angle

Table 2. NMR Data for the (4R,5R)-Antillatoxin Isomer (data acquired in DMSO-d_6 at 298 K)

atom no.	δ_H	$^3J_{HH}$ (Hz)	δ_C	HSQMBC (Hz)[a]	T-ROESY[b]
1			169.8		
2a	2.73 (d)	12.2	44.6	1, 3, 4 (7.0), 12 (5.5)	2b (s)
2b	3.13 (d)	12.2		1, 3, 4 (5.1), 12 (6.1)	2a (s), 4 (m), 13 (m)
3			146.7		
4	2.22 (m)		37.6	2, 3, 5, 6 (4.2), 12, 13	14 (m), 13 (s)
5	5.07 (d)	11.1	82.8	3 (2.5), 4, 6, 7 (4.3), 9′ (<1), 13 (1.2), 14 (2.5)	2a (m), 4 (w), 13 (m), 14 (w)
6			129.7		
7	5.90 (s)		135.6	6/8, 5 (7.9), 9 (5.1), 14 (8.1), 15 (3.0)	4 (w), 5 (s), 9 (s), 13 (m), 14 (w), 15 (m)
8			130.0		
9	5.28 (s)		140.7	7 (7.7), 8, 10, 11 (3.7), 15 (9.7), 16 (3.7), 17 (3.7)	13 (w), 14 (s), 15 (w), 11,16,17 (m)
10			32.1		
11	1.11 (s)		30.5	9, 10	
12a	4.87 (s)		111.7	2 (11.4), 4 (4.1)	5 (m), 12b (s), 13 (m)
12b	4.91 (s)			2 (8.2), 4 (10.8)	2b (m), 12a (s)
13	0.83 (d)	6.9	18.3	3, 4, 5	2b (m), 4 (s), 12a (w), 12b (m), 14 (w),
14	1.50 (s)		12.0	5, 6, 7	5 (w), 9 (s), 12′ (m), 13 (w), 15 (w)
15	1.78 (s)		17.2	7, 8, 9	13 (w), 14 (w), 7(m) 11,16,17 (m)
16	1.11 (s)		30.5	9, 10	
17	1.11 (s)		30.5	9, 10	
1′	9.24 (d)	8.9		1, 2′, 11′	2′ (m), 2b (s), 4 (w), 11′ (w)
2′	5.34 (dq)	6.5, 8.2	42.0	1 (<1), 3′, 11′	5′ (m), 11′ (s)
3′			172.6		
4′					
5′	4.41 (d)	10.9	65.2	3′ (<1), 6′, 12′ (5.4), 15′ (2.5), 13′	2′ (m), 13′ (w), 12′ (w), 14′ (m), 15′ (m)
6′			167.6		
7′	8.34 (bd)	9.5		1, 2	2′ (w), 5′ (m), 8′a (m)
8′a	3.47 (dd)	1.5, 18.3	40.2	6′/9′	4 (w), 8′b (s)
8′b	4.35 (dd)	9.6, 18.3		6′/9′	8′a (s)
9′			167.8		
10′					
11′	1.25 (d)	6.6	18.3	2′, 3′	2′ (s), 1′ (w)
12′	2.70 (s)		27.8	3′, 5′,	13′ (m), 14′ (m), 15′ (m)
13′	2.24 (m)		25.5	6′ (2.5)	14′ (m), 15′ (m)
14′	0.88 (d)	6.5	18.5	5′, 13′, 15′	12′ (m), 13′ (m), 15′ (m)
15′	0.80 (d)	6.7	17.8	5′, 13′, 14′	11′ (w), 13′ (m), 14′ (m)

[a] Coupling constants measured using the HSQMBC experiment, utilizing $^1J_{CH}$ values for the peak fitting protocol. [b] The abbreviations are as follows: s = strong, m = medium, w = weak. The numeric values assigned to these letters are described in the text.

parameters. The constrained model, using the MM2* force field, had a minimum energy of 359.69 kJ/mol. The MC search generated a new minimum of 346.25 kJ, which was found three times (Figure 11b). The 20 lowest energy structures were overlaid (Figure 11a), and an rms deviation was calculated using all non-hydrogen atoms. Of the 20 structures used for the calculation, the energy difference between the minimum and structure 20 was 5.23 kJ/mol. The rms deviation for the 20 isomers was 0.64 Å.

Sodium channels represent the molecular target for an important array of clinically useful drugs including local anesthetics, antiarrythmics, anticonvulsants, and neuroprotective agents.[19] These voltage-gated channels also serve as the target for several groups of neurotoxins, which alter channel function by binding to specific receptor sites. There are no less than six distinct neurotoxin receptor sites on the sodium channel, which mediate characteristic effects on ion permeation or voltage-dependent gating.[20] The neurotoxin receptor sites are localized to both extracellular and intramembrane domains of the α-subunit of the VGSC. The receptor sites at which neurotoxins affect gating have been found to be allosterically coupled, which suggests that conformational changes induced by neurotoxin binding alter the equilibrium between resting-open-closed/inactivated states as well as toxin binding affinity at other neurotoxin receptor sites.[20] Such allosteric modulation of sodium channel function is represented by channel activators such as veratridine and the brevetoxins which act at neurotoxin sites 2 and 5, respectively. These toxins bind preferentially and with high affinity to activated sodium channels and shift the conformational equilibrium toward the activated state.[20]

Batrachotoxin (BTX) is another lipid-soluble toxin that acts at site 2 on the sodium channel to stabilize the channel in the open conformation.[21] The specific binding of [³H]BTX is sensitive to conformational changes induced by the binding of toxins to other sites on the α-subunit of VGSC.[22] We have previously shown that ATX allosterically enhanced the specific binding of [³H]BTX to intact CGCs.[8] This effect of ATX on [³H]BTX binding was synergistically augmented by brevetoxin. The strong synergistic interaction of the ATX recognition site with neurotoxin site 5 suggests that these sites may be topologically close and/or conformationally coupled. The results obtained using [³H]-BTX as a probe for sodium channel conformation allowed us to exclude the interaction of ATX with neurotoxin sites 1, 2, 3, and 5. Site 1 is ruled out because tetrodotoxin and saxitoxin bind to the outer vestibule of the pore of the ion channel and allosterically inhibit the binding of [³H]BTX; this is an effect that is antipodal to that of ATX. We were able to rule out sites 2 and 5 inasmuch as these sites display positive allosteric coupling to the ATX site. Neurotoxin receptor site 3, the target for α-scorpion toxins and sea-anemone toxins, was excluded because ATX enhanced [³H]BTX binding in the presence of a maximally effective concentration of sea-anemone toxin. Although we cannot exclude an interaction of ATX with neurotoxin site 4, the target for β-scorpion toxin, it is reasonable to posit that ATX binds to a novel recognition domain on the α-subunit of the VGSC. The relatively small lipotripeptide structure

Table 3. NMR Data for the (4*R*,5*S*)-Antillatoxin Isomer (data acquired in DMSO-d_6 at 298 K)

atom no.	δ_H	$^3J_{HH}$ (Hz)	δ_C	HSQMBC (Hz)[a]	T-ROESY[b]
1			169.4		
2a	2.90 (d)	16.1	40.6	1, 3, 4, 12	2b (s), 1′ (w), 4 (w), 5 (w), 12a (w)
2b	3.04 (d)	16.1		1, 3, 4, 12	2a (s), 12a (m)
3			144.5		
4	2.49 (obs)		42.5	2 (6.0), 3, 5, 6 (2.8), 12 (6.9), 13	4 (s), 12b (m), 13 (m), 14 (m)
5	4.77 (bs)		81.0	3 (4.3), 4, 6, 13 (3.7), 14 (1.7), 7 (4.3), 9′ (1.2)	2a (w), 4 (m), 7 (m), 13 (w), 14 (m)
6			130.4		
7	5.61 (s)		130.4	5 (6.6), 6/8, 14 (8.6), 9 (6.0), 15 (2.5)	5 (m), 9 (m), 8b (w), 13 (m), 15 (m)
8			130.4		
9	5.19 (s)		139.0	7 (7.9), 10, 15, (10.4), 11 (4.6), 16 (4.6), 17 (4.6)	7 (m), 14 (m), 11,16,17 (m)
10			32.1		
11	1.11 (s)		30.5	9, 10	15 (m)
12a	4.94 (s)		117.3	1, 2 (7.0), 3, 4 (10.1)	2a (w), 2b (m), 12b (s)
12b	5.01 (s)			2 (11.0), 3, 4 (6.4)	4 (s), 12a (s), 13 (m)
13	0.90 (d)	7.3	13.9	3, 4, 5	7 (m), 12b (m), 4 (m), 5 (w)
14	1.63 (s)		15.4	5, 6/7	13 (w), 4 (m), 5 (m), 9 (w), 11,16,17 (w)
15	1.72 (s)		17.7	7/8, 9, 10	7 (w), 13 (w), 11,16, 17 (m)
16	1.11 (s)		30.5	9, 10	15 (m)
17	1.11 (s)		30.5	9, 10	15 (m)
1′	8.32 (d)	8.2		2′	2a (w)
2′	4.65 (dq)	6.5, 8.2	42.8	1′, 3	5′ (m), 11′ (m) 14′ (w)
3′			171.2		
4′					
5′	3.92 (d)	9.7	64.7	3′ (2.1), 6′, 12′ (4.3), 13′, 15′ (2.0)	2′ (m), 13′ (w), 7′ (m), 14′ (w), 15′ (m)
6′			168.9		
7′	7.96 (dd)	5.4, 7.3			5′ (m), 8′a (s), 8′b (w)
8′a	3.68 (dd)	4.9, 16.7	41.4	9′, 6′	8′b (s), 13 (m)
8′b	4.16 (dd)	7.1, 16.7		9′, 6′	8′a (s)
9′			167.7		
10′					
11′	1.18 (d)	6.5	17.5	2′, 3′	2′ (s)
12′	2.65 (s)		29.9	3′, 5′	5′ (w), 13′ (m), 14′ (s)
13′	2.21 (m)		26.8		14′ (m), 15′ (m)
14′	0.76 (d)	6.9	18.6	5′, 13′, 15′	5′ (w), 12′ (w), 13′(s), 15′ (m)
15′	1.01 (d)	6.5	20.9	5′, 13′, 14′	13′ (m), 14′ (m)

[a] Coupling constants measured using the HSQMBC experiment, utilizing $^1J_{CH}$ values for peak fitting protocol. [b] The abbreviations are as follows: s = strong, m = medium, w = weak. The numeric values assigned to these letters are described in the text.

of ATX would not be restricted to an extracellular target, as is the case for the β-scorpion toxins, which are composed of 60−65 amino acids.[20]

Given the unique mechanism of action of ATX, we sought to further characterize its pharmacologic actions. The essential role of the asymmetric carbon atoms in ATX was reflected in the stereoselective effects of the ATX enantiomers. Using three distinct functional responses in intact neurons, we found the (4*R*,5*R*)-isomer of ATX (=natural isomer) to be the preferred configuration. The EC$_{50}$ for this diastereomer ranged from 42 to 58 nM in the three assays. The (4*R*,5*R*)-isomer was 31−135 times more potent than the (4*S*,5*S*)-isomer and 89−209 times more potent than the (4*R*,5*S*)-isomer. Thus the (4*R*,5*R*)-configuration is important for creating a molecular topology that is recognized by the acceptor site on the voltage-gated sodium channel alpha subunit.

As observed in Figure 12a, the most active isomer (4*R*,5*R*) appears in profile as an "L" shape with a hydrophobic interior and a cluster of hydrophilic groups on the exterior of the macrocycle. The calculated model suggests that a hydrogen bond (2.0 Å) possibly exists between the glycine NH (H-7′) and the carboxyl terminus (C-1) of the polyketide chain. The (4*S*,5*S*)-isomer also has an "L"-shaped structure (Figure 12c); however, it is inverted with respect to the natural isomer. The lipid tail is pointing into the plane of the page in Figure 10, and most of the electronegative substituents are on the interior face of the macrocycle, in sharp contrast to the (4*R*,5*R*)-isomer. A potential hydrogen bond of 2.0 Å between H-7′ and the carbonyl oxygen of C-1 is also indicated. In contrast, the (4*R*,5*S*)-isomer has an overall extended conformation with

no apparent hydrogen bond interactions (Figure 12b). Interestingly, this isomer has a *cis* amide bond between the alanine and *N*-Me valine residues. Similarly, the (4*S*,5*R*)-isomer has an overall extended structure; however, a slight twist exists in the macrocycle (Figure 12d). This twist in the ring allows H-7′ and the carbonyl oxygen of C-1 to come within 1.9 Å of each other, allowing for a potential hydrogen bond interaction.

It is not possible to draw definitive conclusions as to which molecular features of antillatoxin are responsible for the dramatic variation in biological activity of the four antillatoxin stereoisomers studied here. However, the NMR constrained molecular modeling studies clearly indicate that these four stereoisomers have significantly altered molecular topologies, and hence in a qualitative sense, these structural differences must underlie the observed variations in activity. Two potential caveats are that (1) a minor conformation may be responsible for the biological activity, and (2) organic solvents were used for these NMR studies, and hence, the deduced solution structures of these antillatoxin stereoisomers may not be biologically relevant. The solution structures for the four antillatoxin stereoisomers (Figure 12) represent time-averaged pictures of the major conformation in each case. Hence, it is conceivable that a minor conformer, one not represented by the models derived in this study, is responsible for the observed biological activity. It has recently been shown that the presumption of a single or strongly preferred conformation for a small molecule that contains easily rotated bonds involves risk and should be done with great caution.[23] This point was exemplified in studies of the solution conformation of taxol.[24] In this latter study, it was found that the

Table 4. NMR Data for the (4S,5S)-Antillatoxin Isomer (data acquired in DMSO-d_6 at 298 K)

atom no.	δ_H	$^3J_{HH}$ (Hz)	δ_C	HSQMBC (Hz)[a]	T-ROESY[b]
1			169.8		
2a	2.87 (d)	14.6	41.9	1, 3, 4 (3.6), 12 (5.4)	2b (s)
2b	3.07 (d)	14.6		1, 3, 4 (4.9), 12 (4.2)	2a (s), 1′ (m)
3			146.7		
4	2.97 (dd)	7.0, 10.4	39.1	2 (3.0)[c], 3,5, 6, 13	14 (m), 13 (w)
5	5.02 (d)	10.5	83.4	3 (2.2), 4, 7 (4.7), 13 (0.8), 14 (2.4), 9′ (1.5)	7 (s), 4 (w), 12a (m), 14 (w)
6			128.8		
7	5.93 (s)		135.8	6/8, 5 (7.8), 14 (7.5), 9 (6.0), 15 (3.0)	4 (w), 5 (s), 9 (w)
8			130.2		
9	5.29 (s)		140.5	7 (7.0), 10, 11 (4.3), 15, (9.6), 16 (4.3), 17 (4.3)	7 (w), 14 (w)
10			32.0		
11	1.12 (s)		30.5	9, 10	
12a	4.84 (s)		111.1	2 (6.0), 3, 4 (9.1), 13	5 (m), 12b (s)
12b	4.80 (s)			2 (12.0), 3, 4 (5.0), 13	2a (m), 2b (m), 12b (s)
13	0.82 (d)	7.0	17.3	3, 4, 5	4 (w)
14	1.66 (s)		12.2	5, 6, 7	4 (m), 9 (w)
15	1.79 (s)		17.4	7, 8, 9, 10	9 (w)
16	1.12 (s)		30.5	9, 10	
17	1.12 (s)		30.5	9, 10	
1′	8.64 (d)	8.5			2b (m), 2′ (w)
2′	4.97 (dq)	6.5, 8.6	42.8	3′	1′ (w), 11′ (w), 5′ (m)
3′			171.8		
4′					
5′	4.42 (d)	10.4	64.2	3′ (2.9), 6′, 12′ (4.8), 14′, 15′ (2.3), 13′	2′ (m), 7′ (m), 14′ (w), 15′ (m)
6′			168.2		
7′	7.76 (t)	4.7			5′ (m), 8′a (w), 8′b (w)
8′a	3.98 (dd)	4.39, 17.9	42.2	6′, 9′	8′b (s), 7′ (w)
8′b	3.73 (dd)	5.1, 17.8		6′, 9′	8′a (s), 7′ (w)
9′			166.5		
10′					
11′	1.21 (d)	6.5	17.8	2′, 3′	2′ (w)
12′	2.65 (s)		28.7	3′, 5′	13′ (w), 14′ (s)
13′	2.22 (m)		26.1		14′ (s), 15′ (m)
14′	0.78 (d)	6.9	18.1	5′, 13′, 15′	5′ (w), 13′(s)
15′	0.94 (d)	6.5	19.2	5′, 13′ 14′	5′ (m), 13′ (m), 15′ (m)

[a] Coupling constants measured using the HSQMBC experiment, utilizing $^1J_{CH}$ values for peak fitting protocol. [b] The abbreviations are as follows: s = strong, m = medium, w = weak. The numeric values assigned to these letters are described in the text. [c] This value is a good estimate of the heteronuclear coupling constant. This value was not accurately obtained due to peak shape complications.

major conformation observed in chloroform was inactive, whereas a minor conformer was responsible for the observed biological activity. While our molecular modeling studies with antillatoxin were not carried out in aqueous solution, the use of DMSO for modeling cyclic peptides is common in the literature.[25,26] In addition, it has been argued that the use of organic solvents mimics lipophilic sites in biological systems (e.g., membranes and receptors).[27] Nevertheless, it is clear that alterations in the solution conformation of antillatoxin resulting from changes in C-4 or C-5 stereochemistry are critical to its pharmacologic actions on intact neurons.

Experimental Section

Cerebellar Granule Cell (CGC) Culture. Primary cultures of CGCs were obtained from 8-day-old Sprague–Dawley rats by a previously described method.[28] Cerebella were removed, stripped of their meninges, minced by mild trituration with a Pasteur pipet, and treated with trypsin for 15 min at 37 °C. The cells were then dissociated by two successive trituration and sedimentation steps in soybean trypsin inhibitor- and Dnase-containing isolation buffer, centrifuged, and resuspended in basal Eagle's medium with Earle's salts containing 10% heat-inactivated fetal bovine serum, 2 mM glutamine, 25 mM KCl, and 100 μg/mL gentamicin. CGCs were plated onto poly-L-lysine (MW = 393 000)-coated 96-well (9 mm) clear-bottomed black-well culture plates (Costar) at a density of 9.6×10^4 cells/well and six-well (35 mm) culture dishes (Fisher) at a density of $(2.5-2.75) \times 10^6$ cells/well, respectively, and incubated at 37 °C in a 5% CO_2/95% humidity atmosphere. Cytosine arabinoside (10 μM final concentration) was added after 18–24 h to inhibit replication of non-neuronal

cells. Cells were fed after 7 days in culture (DIC) with 50 μL/mL of a 25 mg/mL dextrose solution.

Cytotoxicity Assays with Cerebellar Granule Cells. CGCs were used for cytotoxicity assay at 10–13 DIC. All assays were carried out in 1% dimethyl sulfoxide (DMSO), which by itself had no effect on neurons. Growth medium was collected and saved, and CGCs were washed twice in 1 mL of Locke's incubation buffer. CGCs were then exposed to ATX in the presence or absence of TTX for 2 h at 22 °C. At the termination of exposure, the incubation medium was collected for subsequent analysis of lactate dehydrogenase (LDH) activity, using the method of Koh and Choi.[29]

Cytotoxicity with Neuro-2a Cells. Toxicity to mouse neuro-2a cells was determined as previously described.[30]

Intracellular Ca^{2+} Monitoring. CGCs grown in 96-well plates were used for intracellular Ca^{2+} ($[Ca^{2+}]_i$) measurements at 10–13 DIC as described previously.[31] Briefly, the growth medium was removed and replaced with dye loading medium (10 μL/well) containing 4 μM fluo-3 AM and 0.04% pluronic acid in Locke's buffer (154 mM NaCl, 5.6 mM KCl, 1.0 mM $MgCl_2$, 2.3 mM $CaCl_2$, 8.6 mM HEPES, 5.6 mM glucose, and 0.1 mM glycine, pH 7.4). After 1 h incubation in dye loading medium, the neurons were washed four times in fresh Locke's buffer (200 μL/well, 22 °C) using an automated cell washer (Labsystems, Helsinki, Finland) and transferred to the fluorescent laser imaging plate reader (FLIPR, Molecular Devices, Sunnyvale, CA) incubation chamber. The final volume of Locke's buffer in each well was 100 μL.

FLIPR operates by illuminating the bottom of a 96-well microplate with an argon laser and measuring the fluorescence emissions from cell-permeant dyes in all 96 wells simultaneously using a cooled CCD camera.[32] In all experiments, a 50 μL volume of ATX was added from the source plate at 25 μL/s, yielding a final volume of 200 μL/culture well with 1%

Table 5. NMR Data for the (4S,5R)-Antillatoxin Isomer (data acquired in DMSO-d_6 at 298 K)

atom no.	δ_H	$^3J_{HH}$ (Hz)	δ_C	HSQMBC (Hz)[a]	T-ROESY[b]
1			170.2		
2a	2.86 (d)	14.9	42.9	1, 3, 4 (3.8), 12 (1.8)	2b (s), 5 (w)
2b	3.31 (obs)			1, 3, 4 (1.0), 12 (5.2)	2a (s),
3			143.9		
4	2.64 (obs)		38.5	2, 3, 5, 6, 12, 13	5 (m), 14 (m), 13 (m)
5	5.09 (bs)		81.2	3 (4.4), 4, 6, 7 (3.4), 9′, 13 (3.2), 14 (2.0)	2a (w), 4 (s), 13 (w), 14 (m)
6			128.4		
7	5.48 (s)		130.0	6, 8, 5 (6.0), 9 (5.0), 14 (8.1), 15 (2.6)	2b (w), 4 (w), 5 (s), 9 (s), 13 (m), 15 (m)
8			130.1		
9	5.18 (s)		139.5	7/8, 10, 11 (3.8), 15 (9.2), 16 (3.8), 17 (3.8)	4 (w), 7 (s), 13 (w), 14 (m), 15 (w), 11,16,17 (m)
10			31.9		
11	1.09 (s)		30.5	9, 10	
12a	4.98 (s)		116.0	2 (10.9), 4 (4.9)	4 (w), 14 (m), 13 (m)
12b	5.02 (s)			2 (6.6), 4 (9.4)	2a (s), 4 (w), 14 (w)
13	0.86 (d)	7.4	12.7	3, 4, 5	2b (w), 4 (m), 5 (w), 7 (w), 12b (w)
14	1.59 (s)		14.8	5, 6, 7	2b (w), 4 (m), 5 (w), 9 (m)
15	1.72 (s)		17.7	7, 8, 9	4 (w), 7 (m), 9 (w), 11,16,17 (w)
16	1.01 (s)		30.5	9, 10	
17	1.01 (s)		30.5	9, 10	
1′	8.56 (d)	8.8		1, 2′, 11′	2′ (w), 2b (m), 11′ (w)
2′	5.10 (dq)	6.8, 8.8	42.6	1 (3.1), 3′, 11′	1′ (w), 5′ (m), 11′ (m)
3′			172.0		
4′					
5′	4.23 (d)	10.5	64.7	3′ (3.1), 6′, 12′ (6.0), 13′, 14′ (4.9), 15 (4.5)	2′ (m), 13′ (w), 7′ (w), 14′ (w), 15′ (w)
6′			168.3		
7′	8.48 (dd)	3.0, 8.1		1, 2	2′ (w), 5′ (m), 8′a (m)
8′a	3.65 (dd)	3.1, 17.4	41.4	6′/9′	8′b (s)
8′b	4.24 (dd)	8.2, 17.6		6′/9′	8′a (s)
9′			167.7		
10′					
11′	1.20 (d)	6.5	17.4	2′, 3′	2′ (m)
12′	2.65 (s)		28.7	3′, 5′,	13′ (w)
13′	2.23 (m)		26.4	6′ (3.6)	12′ (m), 14′ (s), 15′ (s)
14′	0.75 (d)	6.7	18.3	5′, 13′, 15′	5′ (w), 12′ (m), 13′ (s), 15′ (m)
15′	0.94 (d)	6.5	19.2	5′, 13′, 14′	5′ (m), 13′ (s), 14′ (m)

[a] Coupling constants measured using the HSQMBC experiment, utilizing $^1J_{CH}$ values for peak fitting protocol. [b] The abbreviations are as follows: s = strong, m = medium, w = weak. The numeric values assigned to these letters are described in the text.

DMSO. Neurons were excited by the 488 nm line of the argon laser, and Ca^{2+}-bound fluo-3 emission in the 500−560 nm range was recorded with the CCD camera with shutter speed set at 0.4 s. Fluorescence readings were taken every 10 s during the 3 min prior to ATX addition, then once per second for 75 s following ATX exposure and every 30 s thereafter to the programmed termination of the experiment. Background fluorescence was automatically subtracted from all fluo-3 fluorescence measurements.

Extracellular Acidification Rate by Microphysiometry. To assess the influence of ATX isomers on the metabolic activity of CGC, neurons were seeded into microphysiometer (Cytosensor, Molecular Devices Corp., Sunnyvale, CA) capsule cups and cultured as described above. On the day of the experiment the cell capsules were transferred to the sensor chambers of the microphysiometer, where they were perfused (100 μL/min) with low-buffering RPMI and equilibrated for 30 min to allow stabilization of extracellular pH. The microphysiometer uses a light-addressable silicon sensor to detect extracellular protons.[33] The acidification of the extracellular milieu is due to extrusion of H^+, lactic acid, and carbon dioxide. The extracellular acidification rates were measured during 30 s pauses in the perfusion of chambers, which allows for accumulation of protons and acidic metabolites with attendant reduction in pH. These data are collected as the extracellular acidification rate is μV/s, which represents approximately a milli-pH unit per min. These values were then expressed as a percentage of the baseline determined by computerized analysis of five time points prior to exposure of neurons to ATX isomers. Neurons were exposed to ATX for five stop−start cycles of 90 s each, which were controlled by programmable software (Cytosoft).

Data Analysis of Cerebellar Granule Cell-Based Assays. All experiments were performed with triplicate to quadruplicate determinations and repeated with different cultures. Concentration−response data were fitted by a four-parameter logistic equation using commercially available software (Prism, GraphPad Software, San Diego, CA).

Goldfish Toxicity Assays. Toxicity assays to the common goldfish (*Carassius auratus*) were performed as previously described.[34]

NMR Measurements. All NMR data were recorded on a Bruker DRX spectrometer operating at 600.03 MHZ. Spectra were acquired at 298 K in 99.96% DMSO-d_6. Two milligrams of each of the four stereoisomers were individually dissolved in 0.4 mL of DMSO-d_6 (9.9 mM) and transferred to a Shegemi microcell matched to deuterated DMSO. The spectrometer was equipped with a 5 mm Bruker Q-Switch TXI probe. The ^1H and ^{13}C 90° pulse widths, at a 0 db power level (−6 db maximum), were 9.42 and 14.2 μs, respectively. For the DPFGSE 1D NOE experiment, a 60 ms Gaussian-shaped pulse at 69 db was used for selective irradiation. This experiment was acquired with 1024 scans with 32K data points and processed with 3.0 Hz line broadening with zero-filling to 64K. The HSQMBC experiment was optimized for an 8 Hz (31.2 ms) long-range heteronuclear coupling. A total of 188 scans per 256 increments were acquired with 2K data points in F_2. The data were processed to 4K data points in F_2 and linear predicted to 512 followed by zero-filling to 1K in the F_1 dimension. The spin-lock pulse in the T-ROESY experiment was set at 400 ms. A 90°-shifted cosine function was applied to both dimensions. The data matrix was zero-filled to 1024 × 1024 data points.

Molecular Modeling. All calculations were performed on either an SGI INDY running IRIX 6.3 or a NEC 266 MHz Pentium running SuSE Linux (2.2.14 kernel). The software used in the calculations was Macromodel 7.0. The MM2* force field was used for all minimizations and Monte Carlo conformation searching. The steepest descent (SD) minimization method was used for obtaining the correct starting geometries

of the bonds. Distance restraints were then applied to the model from within the minimization menu of the Macromodel software. This constrained structure was then energy minimized using the PRCG method with 1000 iterations. Torsion angle restraints were added on the basis of the bond angles derived from applying the $^3J_{CH}$ coupling constants to the appropriate Karplus equation. An error of $\pm20°$ was tolerated for these restraints. This structure was then minimized using a 1000 iteration PRCG method. The resulting structure was then subjected to a Monte Carlo conformation search to more thoroughly explore the conformational space allowed by the distance and torsion angle restraints. A 1000-step conformation search was done. Of the structures generated, the 20 lowest energy structures were overlaid and an rms was calculated. The new minimum generated during the search was found multiple times for each isomer.

References and Notes

(1) Gerwick, W. H.; Tan, L. T.; Sitachitta, N. In *The Alkaloids*; Cordell, G. A., Ed.; Academic Press: San Diego, 2001; Vol. 57, pp 75–184.
(2) Verdier-Pinard, P.; Lai, J.-Y.; Yoo, H.-D.; Yu, J.; Marquez, B.; Nagle, D. G.; Nambu, M.; White, J. D.; Falck, J. R.; Gerwick, W. H.; Day, B. W.; Hamel, E. *Mol. Pharmacol.* **1998**, *53*, 62–76.
(3) Wu, M.; Okino, T.; Nogle, L. M.; Marquez, B. L.; Williamson, R. T.; Sitachitta, N.; Berman F. W.; Murray, T. F.; McGough, K.; Jacobs, R.; Colsen, K.; Asano, T.; Yokokawa, F.; Shioiri, T.; Gerwick, W. H. *J. Am. Chem. Soc.* **2000**, *122*, 12041–12042.
(4) Marquez, B. L.; Watts, K. S.; Yokochi, A.; Roberts, M. A.; Verdier-Pinard, P.; Jimenez, J. I.; Hamel, E.; Scheuer, P. J.; Gerwick, W. H. *J. Nat. Prod.* **2002**, *65*, 866–871.
(5) Luesch, H.; Yoshida, W. Y.; Moore, R. E.; Paul, V. J.; Corbett, T. H. *J. Am. Chem. Soc.* **2001**, *123*, 5418–5423.
(6) Orjala, J.; Nagle, D. G.; Hsu, V.; Gerwick, W. H. *J. Am. Chem. Soc.* **1995**, *117*, 8281–8282.
(7) Berman, F. W.; Murray, T. F.; Gerwick, W. H *Toxicon* **1999**, *37*, 1645–1648.
(8) Li, W. I.; Berman, F. W.; Okino, T.; Yokokawa, F.; Shioiri, T.; Gerwick, W. H.; Murray, T. F. *Proc. Natl. Acad. Sci. U.S.A.* **2001**, *98*, 7599–7604.
(9) Yokokawa, F.; Fujiwara, H.; Shioiri, T. *Tetrahedron* **2000**, *56*, 1759–1775.
(10) Stott, K.; Stonehouse, J.; Keeler, J.; Hwang, T.-L.; Shaka, A. J. *J. Am. Chem. Soc.* **1995**, *117*, 4199–4200.
(11) Willker, W.; Liebfritz, D.; Kerssebaum, R.; Lohman, J. *J. Magn. Reson. Ser. A* **1993**, *102*, 348–350.
(12) Williamson, R. T.; Marquez, B. L.; Kover, K. E.; Gerwick, W. H. *Magn. Reson. Chem.* **2000**, *38*, 265–273.
(13) Hwang, T.-L.; Shaka, A. J. *J. Magn. Reson. Ser. B* **1993**, *102*, 155–165.
(14) Ludvigsen, S.; Andersen, K. V.; Poulsen, F. M. *J. Mol. Biol.* **1991**, *217*, 731–736.
(15) Kao, L.-F.; Barfield, M. *J. Am. Chem. Soc.* **1985**, *107*, 2323–2330.
(16) Haasnoot, C. A. G.; DeLeeuw, F. A. A. M.; Altona, C. *Tetrahedron* **1980**, *36*, 2783–2792.
(17) Mohamadi, F.; Richards, N. G. J.; Guida, W. C.; Liskamp, R.; Lipton, M.; Caufield, C.; Chang, G.; Hendrickson, T.; Still, W. C. *J. Comput. Chem.* **1990**, *11*, 440–462.
(18) Polak, E.; Ribier, G. *Rev. Fr. Inf. Rech. Oper.* **1969**, *16*, 35–43.
(19) Taylor, C. P.; Meldram, B. S. *Trends Pharmacol. Sci.* **1995**, *16*, 309–316.
(20) Cestele, S.; Catterall, W. A. *Biochimie* **2000**, *82*, 883–892.
(21) Wang, S. Y.; Barile, M.; Wang, G. K. *Mol. Pharmacol.* **2001**, *59*, 1100–1107.
(22) Catterall, W. A.; Morrow, C. S.; Daly, J. W.; Brown, G. B. *J. Biol. Chem.* **1981**, *256*, 8922–8927.
(23) Nevins, N.; Cicero, D.; Snyder, J. P. *J. Org. Chem.* **1999**, *64*, 3979–3986.
(24) Snyder, J. P.; Nevins, N.; Cicero, D. O.; Jansen, J. *J. Am. Chem. Soc.* **2000**, *122*, 724–725.
(25) Inman, W.; Crews, P. *J. Am. Chem. Soc.* **1989**, *111*, 2822–2829.
(26) Morita, H.; Kayashita, T.; Takeya, K.; Itokawa, H.; Shiro, M. *Tetrahedron* **1997**, *53*, 1607–1616.
(27) Behrens, S.; Matha, B.; Bitan, G.; Gilon, C.; Kessler, H. *Int. J. Pept. Protein Res.* **1996**, *48*, 569–579.
(28) Berman, F. W.; Murray, T. F. *J. Biochem. Toxicol.* **1996**, *11*, 111–119.
(29) Koh, J. Y.; Choi, D. W. *J. Neurosci. Methods* **1987**, *20*, 83–90.
(30) Manger, R. L.; Leja, L. S.; Lee, S. Y.; Hungerford, J. M.; Hokama, Y.; Dickey, R. W.; Granade, H. R.; Lewis, R.; Yasumoto, T.; Wekell, M. M. *JAOAC Int.* **1995**, *78*, 521–527.
(31) Berman, F. W.; Murray, T. F *J. Neurochem.* **2000**, *74*, 1443–1451.
(32) Schroeder, K. S.; Neagle, B. D. *J. Biomol. Screen.* **1996**, *1*, 75–80.
(33) McConnell, H. M.; Owicki, J. C.; Parce, J. W.; Miller, D. L.; Baxter, G. T.; Wada, H. G.; Pritchford, S. *Science* **1992**, *257*, 1906–1912.
(34) Orjala, J.; Nagle, D.; Gerwick, W. H. *J. Nat. Prod.* **1995**, *58*, 764–768.

NP0303409